Observational and Model Evidence for Positive Low-Level Cloud Feedback

Amy C. Clement *et al.*

Science **325**, 460 (2009);
DOI: 10.1126/science.1171255

Science (print ISSN 0036-8075; online ISSN 1095-9203) is published weekly, except the last week in December, by the American Association for the Advancement of Science, 1200 New York Avenue NW, Washington, DC 20005.

deformation of opposite sign until square. The elastic energy $f_E(\sigma', \sigma'')$ of the resulting laminate of half-layers in a given state of curvature was then calculated to quadratic order in the principal curvatures σ' and σ''. The layer elastic energy per volume obtained is $f_E = K/2(\sigma' + \sigma'')^2 - \bar{K}(\sigma'\sigma'') + G(\sigma'' - \sigma')$, where K is the Frank elastic constant for mean curvature $(\sigma' + \sigma'')$, $\bar{K}$ is the Frank constant for Gaussian curvature $(-\sigma'\sigma'')$, and $G \propto \beta$ drives curvature in response to the frustrated internal in-plane layer strain β (*16*). For a minimal surface ($\sigma = \sigma' = -\sigma''$), the free energy is particularly simple: $f_E^m = \bar{K}\sigma^2 - 2G\sigma$, making $R_p \equiv \bar{K}/G$ the preferred radius of curvature. The energy $f = f_E(\sigma', \sigma'') + \Delta u$, where Δu is the Gibbs potential per volume of the in-plane freezing, can be used to predict the structure of a filament, viewed as a set of ribbon-like layers twisted with a half-pitch $h \equiv \pi/q$ (*16*). The central layer is a minimal surface of curvature $\sigma = q$ along its centerline, so that for a very narrow ribbon ($w << h$), minimizing f_E^m gives $q = G/\bar{K}$ and therefore $h = \pi/\sigma_p = \pi R_p \sim 20$ nm. However, as T is lowered into the B4 range, the ribbon can further lower its free energy by growing wider, gaining Δu in a larger volume. Overall energy minimization yields finite-width filaments with the layer ordering suppressed (melted) outside, as the increase in w is ultimately limited by the energy cost of reduced (and thus less favorable) curvature away from the centerline in a wider ribbon. Predicted values of w and h are consistent with $R_p \sim 200$ nm, about 4 times the estimate from the in-layer structure (*16*).

The orientation of the in-plane structure within the nanofilaments is shown in Fig. 4, F to H, and fig. S4M. The lattice diagonal (polarization **p**) must be either along or normal to the NF axis for the saddle splay curvature to give the required NF twist (Fig. 4, E and F). The choice of **p** to be along the NF axis is clearly indicated by second harmonic generation (SHG) evidence for local C_∞ rather than D_∞ symmetry of the phase (*16*, *24*). With this orientation, the filament edges are (1,1) rows of molecules (fig. S4M); the result is a crystal face with a low Miller index that resists the addition of new material upon cooling, thereby promoting the highly anisotropic growth of the needle-like filaments.

Upon slow cooling into the B4 phase, the filaments appear via heterogeneous nucleation at dilute sites. Each nucleation site is homochiral; FFTEM and AFM show that once a handedness is chosen, single-handed domains are formed, out to distances of 10 to 100 μm. This leads to the observed strong "sergeants and soldiers" enantioselection of B4 chirality by weak chiral doping (*18*), chiral surface treatment (*25*), or nucleation from a chiral phase (*14*). At higher temperatures the NF phase is fluid, likely a consequence of lubrication of the filaments by the B2 or isotropic phase that is suppressed from hexatic ordering by the requirement for layer curvature. This fluidity enables the filaments to anneal in their orientation and twist phase into the coherent helical structures seen in Fig. 2G, Fig. 3, and fig. S1. Such coherence shows that the filaments must interact, but this interaction is weak in that it does not noticeably influence the structure of contacting filaments (Fig. 2, E and F). The AFM textures like that in Fig. 3E, visualizing the planes nearly normal to **p**, suggest that this interaction is strongest when layers in adjacent filaments are face-to-face and provide unambiguous evidence for the coherent macroscopic helical twist of the layering.

The B4 or HNF phase appears in a simple bent-core molecular system as a response to the competition between layering and twist inherent in chiral media. The inability of the best local solution to fill space selectively suppresses layering to produce a nanophase segregation of different degrees of order in a structural hierarchy that enables both macroscopic chirality and layering in an exotic liquid crystal phase.

References and Notes

1. J. F. Annett, *Superconductivity, Superfluids, and Condensates* (Oxford Univ. Press, Oxford, 2004).
2. M. Seul, D. Andelman, *Science* **267**, 476 (1995).
3. A. H. de Vries, S. Yefimov, A. E. Mark, S. J. Marrink, *Proc. Natl. Acad. Sci. U.S.A.* **102**, 5392 (2005).
4. D. A. Coleman *et al.*, *Science* **301**, 1204 (2003).
5. P. G. deGennes, *Solid State Commun.* **10**, 753 (1972).
6. S. R. Renn, T. C. Lubensky, *Phys. Rev. A* **38**, 2132 (1988).
7. J. Fernsler *et al.*, *Proc. Natl. Acad. Sci. U.S.A.* **102**, 14191 (2005).
8. T. Sekine *et al.*, *J. Mater. Chem.* **7**, 1307 (1997).
9. T. Sekine *et al.*, *Jpn. J. Appl. Phys.* **36**, 6455 (1997).
10. P. Collings *et al.*, *Abstracts of the First International Workshop on Banana-Shaped Liquid Crystals*, Berlin (1997) (www2.tu-berlin.de/~insi/ag_heppke/banana).
11. D. M. Walba, L. Eshdat, E. Korblova, R. K. Shoemaker, *Cryst. Growth Des.* **5**, 2091 (2005).
12. H. Takezoe, Y. Takanishi, *Jpn. J. Appl. Phys.* **45**, 597 (2006).
13. R. A. Reddy, C. Tschierske, *J. Mater. Chem.* **16**, 907 (2006).
14. H. Niwano *et al.*, *J. Phys. Chem. B* **108**, 14889 (2004).
15. J. Thisayukta, H. Takezoe, J. Watanabe, *Jpn. J. Appl. Phys.* **40**, 3277 (2001).
16. See supporting material on *Science* Online.
17. T. Niori, T. Sekine, J. Watanabe, T. Furukawa, H. Takezoe, *J. Mater. Chem.* **6**, 1231 (1996).
18. D. R. Link *et al.*, *Science* **278**, 1924 (1997).
19. A. Aggeli *et al.*, *Proc. Natl. Acad. Sci. U.S.A.* **98**, 11857 (2001).
20. M. S. Spector, J. M. Schnur, J. V. Selinger, in *Materials Chirality: A Special Volume in the Topics in Stereochemistry Series*, M. M. Green, R. J. M. Nolte, E. W. Meijer, Eds. (Wiley-VCH, Weinheim, Germany, 2002), pp. 281–372.
21. R. G. Weiss, P. Terech, *Molecular Gels: Materials with Self-Assembled Fibrillar Networks* (Springer, Dordrecht, Netherlands, 2005).
22. J. Thisayukta *et al.*, *J. Am. Chem. Soc.* **122**, 7441 (2000).
23. W. L. Noorduin *et al.*, *J. Am. Chem. Soc.* **130**, 1158 (2008).
24. F. Araoka *et al.*, *Phys. Rev. Lett.* **94**, 137801 (2005).
25. S.-W. Choi *et al.*, *Angew. Chem. Int. Ed.* **45**, 6503 (2006).
26. Y. Bouligand, F. Livolant, *J. Phys.* **45**, 1899 (1984).

27. Supported by NSF grant DMR 0606528 (N.A.C.), NSF Materials Research Science and Engineering Center grant DMR 0820579 (N.A.C.), an NSF Graduate Research Fellowship (L.H.), Deutsche Forschungsgemeinschaft grant Sfb 448 (J.P.R.), and NIH grant HL-51177 (J.Z.). Use of the National Synchrotron Light Source was supported by the U.S. Department of Energy, Divisions of Materials and Chemical Sciences.

Supporting Online Material

www.sciencemag.org/cgi/content/full/325/5939/456/DC1
Materials and Methods
SOM Text
Figs. S1 to S8
References

19 December 2008; accepted 4 June 2009
10.1126/science.1170027

Observational and Model Evidence for Positive Low-Level Cloud Feedback

Amy C. Clement,[1]* Robert Burgman,[1] Joel R. Norris[2]

Feedbacks involving low-level clouds remain a primary cause of uncertainty in global climate model projections. This issue was addressed by examining changes in low-level clouds over the Northeast Pacific in observations and climate models. Decadal fluctuations were identified in multiple, independent cloud data sets, and changes in cloud cover appeared to be linked to changes in both local temperature structure and large-scale circulation. This observational analysis further indicated that clouds act as a positive feedback in this region on decadal time scales. The observed relationships between cloud cover and regional meteorological conditions provide a more complete way of testing the realism of the cloud simulation in current-generation climate models. The only model that passed this test simulated a reduction in cloud cover over much of the Pacific when greenhouse gases were increased, providing modeling evidence for a positive low-level cloud feedback.

Low-level clouds are of great climatic importance because of their net cooling effect on the global climate (*1*). If the coverage of this type of cloud were to change as the climate warms, it could lead to either an enhancement or a reduction in the warming (i.e., as either a positive or negative feedback, depending on whether cloud cover decreases or increases). At

present, the sign of the low-level cloud feedback in climate change is unknown (*2*–*5*).

Previous research on the subtropical stratocumulus decks in the Northeast (NE) Pacific has laid the groundwork for our current understanding of environmental controls on this cloud type (*6*–*10*). These studies have shown that changes in local meteorological conditions can explain much of the variability in low-level cloud cover occurring on daily to interannual time scales. The longer-term variability of these clouds, however, has received much less attention, partly because long-term fluctuations in any particular cloud data set would rightly be regarded with some skepticism. Surface-based cloud observations, for instance, can be problematic due to the subjective nature of the measurement and sparse sampling for large regions of the ocean (*11*, *12*). Satellite-based cloud observations have spurious trends related to instrument drift and calibration (*13*, *14*) and are available for only the past 25 years. Here we examine long-term cloud variations in independent cloud data sets and analyze meteorological data to provide a physical framework for interpreting these variations.

Our principal source of data is monthly mean gridded surface-based observations of total cloud cover from the Comprehensive Ocean Atmosphere Data Set (*15*) (COADS) during 1952 to 2007. We supplement this with cloud-type information from COADS that has been compiled by Hahn and Warren (*16*) for the period 1952 to 1997, and in particular, we examine the category of marine stratiform clouds (comprising ordinary stratocumulus, cumulus under stratocumulus, fair-weather stratus, and bad-weather stratus). Additional independent information on total cloud amount, low-level cloud amount, and surface radiative fluxes is provided by the International Satellite Cloud Climatology Project (*17*, *18*) (ISCCP). Before using ISCCP data, we applied some adjustments to remove spurious long-term variability caused by satellite artifacts and to account for erroneous retrievals of low-level cloud-top height (*19*). Other climate variables used in the analysis are sea surface temperature (SST) (*20*), sea-level pressure (SLP) from the Hadley center reanalysis (*21*), and vertical velocity, surface winds, and lower tropospheric static stability (potential temperature at 700 mb minus surface temperature) from the ERA-40 reanalysis (*22*).

The time series of total and low-level cloud cover averaged over the NE Pacific (115° to 145°W, 15° to 25°N) are displayed in Fig. 1, A and B. Both COADS and adjusted ISCCP data sets show a shift toward more total cloud cover in the late 1990s, and the shift is dominated by low-level cloud cover in the adjusted ISCCP data (bars, in Fig. 1B). The longer COADS total cloud time series indicates that a similar-magnitude shift toward reduced cloud cover occurred in the mid-1970s, and this earlier shift was also dominated by marine stratiform clouds (bars, Fig. 1A). PATMOS-X, a next-generation version (*23*) of the Advanced Very High Resolution Radiometer Pathfinder Atmosphere (PATMOS) data set with improved algorithms (*24*), shows similar signals over the 1982 to 2007 period (fig. S1). These cloud changes appear throughout the year, and the shifts are also apparent in SST and SLP time series (Fig. 1, C and D).

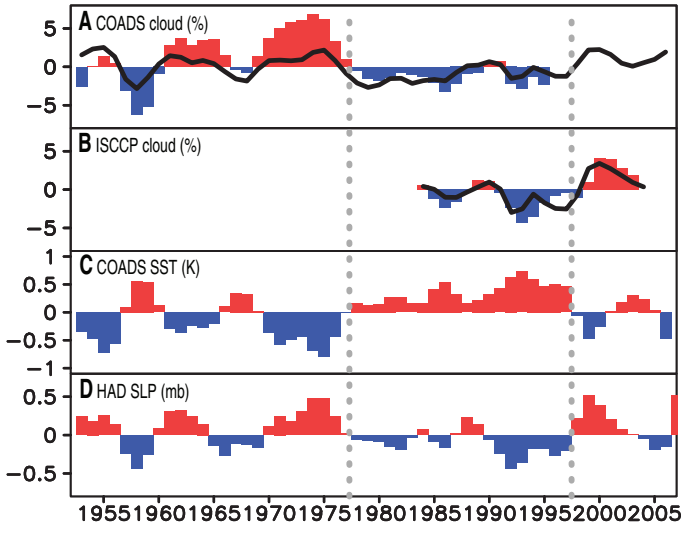

Fig. 1. Time series of annual mean values of cloud and climate quantities averaged over the NE Pacific (115° to 145°W, 15° to 25°N). The time mean of each field is removed, and a 1-2-1 smoothing is applied. (**A**) COADS total cloud cover (black line) and marine stratiform cloud cover (bars). Units are percent cloud cover. (**B**) Adjusted ISCCP total cloud cover (black line) and adjusted ISCCP low- plus mid-level cloud cover (bars). Units are percent cloud cover. (**C**) COADS SST. Units are K. (**D**) Hadley center SLP. Units are hPa. The vertical dashed lines indicate the approximate mid-point of the 1976 and 1990s climate shifts that have been previously identified in the literature. We use low- plus mid-level cloud cover from ISCCP rather than low-level only because low-level clouds can be mistakenly identified as mid-level clouds. This does not appear to be as much of an issue in the NE Pacific as it is for the SE Pacific (*19*).

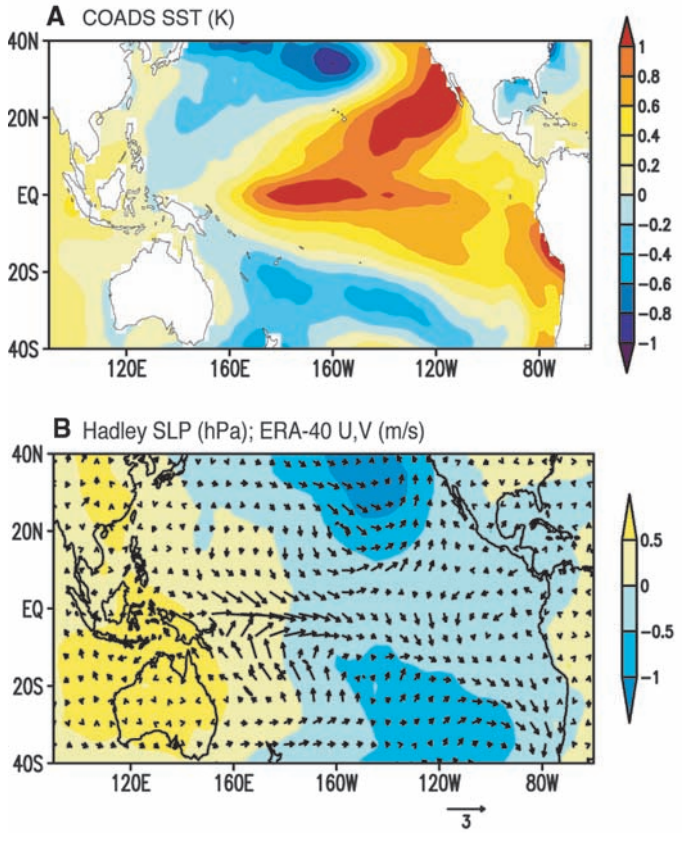

Fig. 2. Regression of climate variables on the time series of NE Pacific SST (from Fig. 1C). Values are shown per degree change in the NE Pacific index. (**A**) SST (in K). (**B**) SLP (colors, units of hPa), surface winds from ERA-40 (arrows, units of m/s).

[1]Rosenstiel School of Marine and Atmospheric Sciences, University of Miami, Division of Meteorology and Physical Oceanography, MSC 362, 4600 Rickenbacker Causeway, Miami, FL 33149, USA. [2]Scripps Institution of Oceanography, University of California-San Diego, La Jolla, CA 92093–0224, USA.

*To whom correspondence should be addressed. E-mail: aclement@rsmas.miami.edu

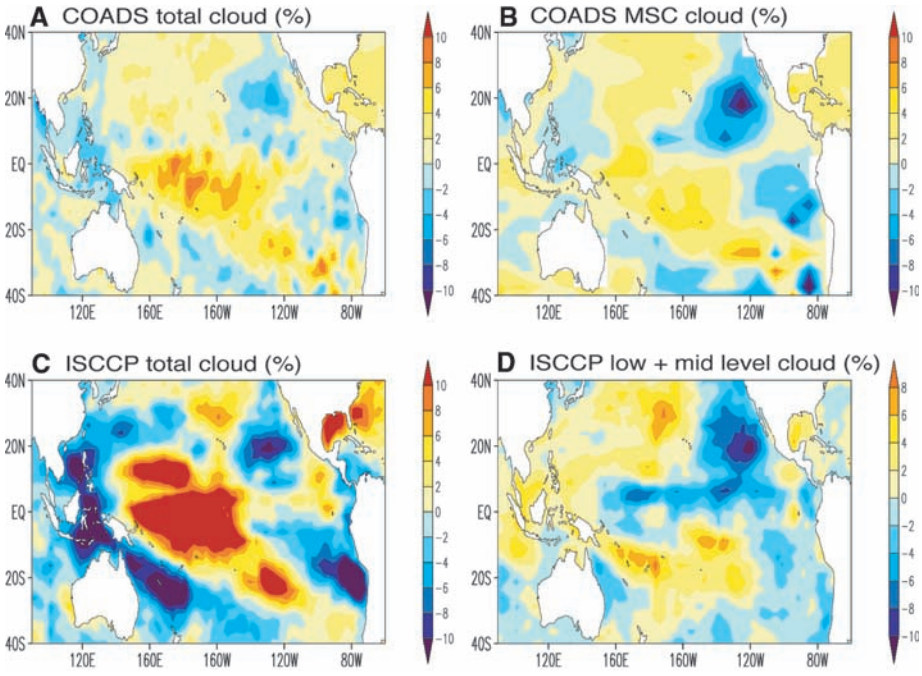

Fig. 3. Regression of cloud data on the time series of NE Pacific SST (from Fig. 1C). All panels are in units of percent cloud cover per degree change in the SST index. (**A**) COADS total cloud cover (for the period 1952 to 2006). (**B**) COADS marine stratiform cloud (MSC) cover (for the period 1952 to 1997). (**C**) Adjusted ISCCP total cloud and (**D**) adjusted ISCCP low- plus mid-level cloud cover [both (C) and (D) are for the period 1984 to 2005].

Table 1. Correlation between cloud and various meteorological quantities in the NE Pacific for observations and climate models. For the observations, the ISCCP-corrected and COADS cloud fraction (both total and low-level cloud values are shown) are correlated with observed SST (first column), lower tropospheric stability (LTS, second column), sea-level pressure (SLP, third column), and mid-tropospheric pressure vertical velocity (fourth column). For the models, the total cloud cover is used because the separate low-level cloud cover is not made available in this archive for most models. Models are grouped according to the sign of the correlation (*r*) relative to observations. We only include models for which all diagnostics are available. Statistical significance of the correlation values is calculated with a one-tailed *t* test. Degrees of freedom are derived with the lag-1 autocorrelation. Values that are significant at the 99% level are shown in bold.

	SST	LTS	SLP	ω 500
Observations				
ISSCP-corrected total	**-0.75**	0.44	**0.80**	0.30
ISCCP-corrected low + mid	**-0.91**	**0.81**	**0.89**	**0.70**
COADS total	**-0.74**	0.35	**0.73**	0.53
COADS MSC	**-0.82**	0.42	**0.74**	**0.70**
Models with the correct cloud-meteorology relationships				
ukmo_hadgem1	**-0.81**	**0.84**	**0.65**	**0.39**
inmcm3_0	**-0.77**	**0.37**	**0.58**	0.14
Models that simulate the wrong sign r(cloud, ω 500)				
mri_cgcm2_3_2a	**-0.60**	0.21	**0.35**	**-0.58**
gfdl_cm2_0	**-0.69**	0.06	**0.52**	**-0.42**
ncar_ccsm3_0	**-0.66**	**0.48**	**0.63**	-0.18
Models that simulate the wrong sign r(cloud, SLP)				
miroc3_2_hires	**-0.91**	**0.54**	-0.03	-0.10
Models that simulate the wrong sign (or close to zero) r(cloud, LTS)				
cccma_cgcm3_1_t63	**-0.86**	0.01	**0.52**	0.20
cccma_cgcm3_1	**-0.80**	-0.08	**0.35**	-0.14
cnrm_cm3	**-0.73**	-0.24	**0.54**	**-0.54**
ipsl_cm4	**-0.53**	-0.16	0.25	**-0.32**
ukmo_hadcm3	**-0.44**	-0.17	**0.33**	**-0.43**
gfdl_cm2_1	**-0.31**	**-0.38**	0.05	**-0.56**
mpi_echam5	-0.23	**-0.44**	0.06	**-0.70**
miroc3_2_medres	-0.13	-0.08	-0.04	**-0.67**
Models that simulate the wrong sign r(cloud, SST)				
giss_aom	0.12	**-0.63**	**-0.39**	**-0.67**
iap_fgoals1_0_g	0.22	**-0.43**	-0.24	**-0.89**
giss_model_e_h	0.34	0.10	0.10	**-0.81**
giss_model_e_r	**0.39**	-0.04	0.003	**-0.58**

The decadal changes in NE Pacific clouds and climate are linked to well-known basin-wide climate shifts (*25*–*30*). This is illustrated in Fig. 2, A and B, which shows that the regression patterns of SST, SLP, and ERA-40 surface winds on the NE Pacific SST time series resemble the now familiar pattern of Pacific Decadal Variability. The SST signal spans the entire Pacific basin and persists throughout the year, and the SLP pattern comprises a weaker Walker circulation in the equatorial region and a deeper Aleutian low in the North Pacific (Fig. 2B). The extension of the North Pacific SLP low anomaly into the stratocumulus region constitutes a weakening of the climatological high, and trade winds around the high are weakened (hence the anomalous southerly and westerly flow shown in Fig. 2B). The subsidence and lower tropospheric stability (LTS) in the NE Pacific are both weaker when SST is warm there (fig. S2).

The spatial patterns of cloud-cover change (Fig. 3) are physically consistent with the local meteorological changes displayed in Fig. 2 and fig. S2, with reduced cloud cover in the NE Pacific when SST is warm, SLP is low, and subsidence, equatorward advection, and static stability are weak (*6*–*10*). For COADS total cloud, we calculate the regression over the entire time period (Fig. 3A), which includes both the 1976 and late-1990s shifts. The regression for marine stratiform cloud (Fig. 3B), however, includes only the 1976 shift due to lack of the Hahn and Warren data compilation after 1997. A comparison of the patterns in Fig. 3, A and B, indicates that marine stratiform cloudiness dominates the total cloud cover change and that the climate shifts in 1976 and the late 1990s were analogous but of opposite sign (i.e., the

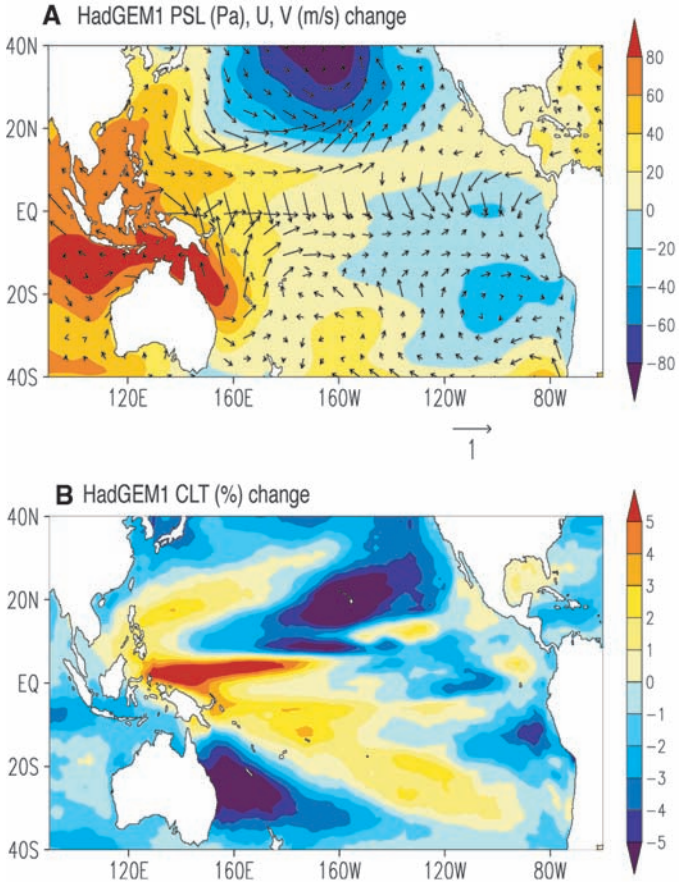

Fig. 4. (**A**) UKMO-HadGEM1 sea-level pressure change in 2 × CO_2 – present climate (in Pa). (**B**) Total cloud cover (CLT) change (%) in UKMO-HadGEM1 for 2 × CO_2 – present climate. These data are taken from the 1pctto2x experiment, which was initialized from year 410 of the PIcntrl experiment. CO_2 was increased by 1% per year, compounded until doubling (year 480), and then held fixed [at 710 parts per million (ppm)] for another 150 years. The differences shown in this figure were calculated by taking the last 50 years of the simulation with CO_2 held at 710 ppm and subtracting years 1 to 70 of the simulation.

earlier shift was a warming and reduction in clouds and the latter a cooling and increase in clouds). The adjusted ISCCP regressions for total and low-level cloud (Fig. 3, C and D) are in agreement with both total and marine stratiform cloudiness from COADS. This concurrence is surprising given the fundamentally different measurement methods (human eye versus satellite retrieval and algorithm). Furthermore, the similarity in pattern and magnitude between adjusted ISCCP low-level cloud cover and the COADS marine stratiform cloud cover is especially impressive considering that they do not occur over the same climate shifts (adjusted ISCCP captures only the late-1990s shift, whereas COADS marine stratiform captures only the 1976 shift). The larger size of both COADS and adjusted ISCCP low-level cloud signals relative to the total cloud signals in the NE Pacific indicates that upper-level clouds increase when low-level clouds decrease. Enhanced upper-level cloud cover is consistent with the weakening of subsidence over the NE Pacific (fig. S2).

We emphasize that the NE Pacific cloud changes described above are tied to cloud changes that span the Pacific basin. Despite much less surface sampling in the Southeast (SE) Pacific, cloud and meteorological changes in that region generally occur in parallel with those in the NE Pacific (Figs. 2 and 3). Also, we find that the leading mode in an empirical orthogonal function analysis (15% of the variance) of global cloud cover (fig. S3) has a spatial pattern similar to that in Fig. 3 and the time series shows the same decadal shifts as in Fig. 1, indicating that the changes in the NE Pacific are part of a dominant mode of global cloud variability.

The regression of adjusted shortwave and longwave cloud radiative effects from the ISCCP Flux Dataset on NE Pacific SST reveals that the change in net cloud radiative effect warms the ocean by about 6 W m^{-2} K^{-1} (fig. S4). Despite the weaker winds, latent heat flux anomalies still act to cool the ocean when SST is warmer (*31*). Model studies have shown a negligible simulated SST response when forced with a wind pattern like that displayed in Fig. 2B (*32*), suggesting that ocean dynamics play little role in NE Pacific decadal SST variability. Hence, we conclude that a change in solar heating of the ocean due to a change in stratocumulus cloud cover is the principal factor maintaining decadal SST anomalies in the NE Pacific. Previous studies have shown that decreased cloud cover and warm SST additionally promote weaker circulation (*33*–*37*). This response is caused by a decrease in longwave radiative cooling of the boundary layer by clouds that reduces large-scale horizontal temperature and pressure gradients. The existence of these same relationships among SST, cloud, and circulation on decadal time scales implies that changes in subtropical stratocumulus act as a positive feedback on climate in the region.

Is this feedback present in climate models? To address this question, we analyze the 20th-century climate simulation in 18 coupled ocean-atmosphere general circulation models with comprehensive output available from the World Climate Research Programme's (WCRP's) Coupled Model Intercomparison Project phase 3 (CMIP3) multimodel archive (*38*, *39*). Correlations between cloud cover in the NE Pacific and the local thermal structure (SST and LTS) and circulation (SLP and mid-tropospheric vertical velocity) are computed for each model and compared with observations in Table 1. Models are grouped according to whether they have the wrong sign correlation relative to observations. By eliminating models successively on this basis, we are left with only two that simulate the correct sign correlations for all variables, the INM-CM3.0 and the HadGEM1. Because these two models represent opposite ends of the range of values of equilibrium climate sensitivity (INM-CM3.0 has the lowest value and HadGEM1 has the highest) (*5*), the cloud-meteorology correlation test alone is not a sufficient metric for global climate sensitivity.

These models are distinct in other ways that are relevant for the simulation of low-level clouds. The INM-CM3.0 adopts a more empirical approach that parameterizes low-level cloud cover as a linear function of relative humidity with coefficients that depend on temperature, altitude, land/ocean, and stratification (*40*), whereas the HadGEM1 has higher spatial resolution, more explicit cloud microphysics, interactive parameterization of cloudiness as a function of local variability in humidity, and a sophisticated planetary boundary-layer mixing scheme (*41*, *42*). Moreover, the HadGEM1 produces doubled carbon dioxide (2 × CO_2) changes in SST, LTS, and circulation that are consistent with the multimodel mean, but the INM-CM3.0 does not (fig. S5). Unlike the INM-CM3.0, most models simulate a weakening of tropical atmospheric circulation under increased greenhouse gases (*43*)—a phenomenon that appears in 20th-century observations as well (*43*, *44*).

Our observational analysis indicates that increased SST and weaker subtropical highs (Fig. 4A) will act to reduce NE Pacific cloud cover, as indeed occurs in HadGEM1 under increased greenhouse gases (Fig. 4B). Although one might expect an increase in low-level cloud cover from the increase in LTS simulated by all models for 2 × CO_2 (*45*, *46*), the resemblance of the spatial structures of the HadGEM1 2 × CO_2 cloud change and SLP change (Fig. 4) to observed decadal cloud and SLP variability suggests that LTS does not play a dominant role. Although we cannot evaluate the exact causes of these cloud changes without additional experiments, the decreased cloud cover in subtropical stratocumulus regions appears to

result from warmer SST and a weakening of the large-scale atmospheric circulation in the Pacific in this model.

The question of whether low-level clouds act as a positive or negative feedback to climate change has been an issue for decades. The analysis presented here provides observational evidence that this feedback is positive in the NE Pacific on decadal time scales. The only model in the CMIP3 archive that properly simulates clouds in the NE Pacific and exhibits $2 \times CO_2$ circulation changes that are consistent with multimodel mean produces a reduction in cloud throughout much of the Pacific in response to greenhouse gas forcing (i.e., a positive feedback). Evaluating cloud feedback with one model is, however, far from ideal. This presents a clear challenge to develop a larger number of climate models that can pass these and other tests so that we may have greater confidence in the sign of the low-cloud feedback under future changes in greenhouse gas concentrations.

References and Notes

1. D. L. Hartmann, M. E. Ockert-Bell, M. L. Michelsen, *J. Clim.* **5**, 1281 (1992).
2. S. Bony, J.-L. Dufresne, *Geophys. Res. Lett.* **32**, L20806 (2005).
3. B. J. Soden, I. M. Held, *J. Clim.* **19**, 3354 (2006).
4. M. J. Webb *et al*., *Clim. Dyn.* **27**, 17 (2006).
5. Intergovernmental Panel on Climate Change, *Climate Change 2007: The Physical Science Basis,* Contribution of Working Group I to the Fourth Assessment Report of the IPCC, S. Solomon *et al*., Eds. (Cambridge Univ. Press, Cambridge, 2007).
6. S. A. Klein, D. L. Hartmann, *J. Clim.* **6**, 1587 (1993).
7. S. A. Klein, D. L. Hartmann, J. R. Norris, *J. Clim.* **8**, 1140 (1995).
8. J. R. Norris, S. A. Klein, *J. Clim.* **13**, 245 (2000).
9. B. Stevens *et al*., *Mon. Weather Rev.* **135**, 985 (2007).
10. J. R. Norris, C. B. Leovy, *J. Clim.* **7**, 1915 (1994).
11. J. R. Norris, *J. Clim.* **12**, 1864 (1999).
12. J. R. Norris, *J. Geophys. Res.* **110**, D08206 (2005).
13. A. T. Evan, A. K. Heidinger, D. J. Vimont, *Geophys. Res. Lett.* **34**, L04701 (2007).
14. J. R. Norris, *Space Sci. Rev.* **94**, 375 (2000).
15. S. J. Worley, S. D. Woodruff, R. W. Reynolds, S. J. Lubker, N. Lott, *Int. J. Climatol.* **25**, 823 (2005).
16. C. J. Hahn, S. G. Warren, "Extended edited synoptic cloud reports from ships and land stations over the globe, 1952-1996," NDP-026C (Carbon Dioxide Information Analysis Center, Oak Ridge National Laboratory, Oak Ridge, TN, 1999); available at http://cdiac.esd.ornl.gov/epubs/ndp/ndp026c/ndp026c.html.
17. W. B. Rossow, R. A. Schiffer, *Bull. Am. Meteorol. Soc.* **80**, 2261 (1999).
18. Y. Zhang, W. B. Rossow, A. A. Lacis, V. Oinas, M. I. Mishchenko, *J. Geophys. Res.* **109**, D19105 (2004).
19. Supporting material is available at *Science* Online.
20. T. M. Smith, R. W. Reynolds, *J. Clim.* **16**, 1495 (2003).
21. R. Allan, T. Ansell, *J. Clim.* **19**, 5816 (2006).
22. S. M. Uppala *et al*., *Q. J. R. Meteorol. Soc.* **131**, 2961 (2006).
23. M. J. Pavolonis, A. K. Heidinger, T. Uttal, *J. Appl. Meteorol.* **44**, 804 (2005).
24. H. Jacobowitz *et al*., *Bull. Am. Meteorol. Soc.* **84**, 785 (2003).
25. C. Deser, A. S. Phillips, J. W. Hurrell, *J. Clim.* **17**, 3109 (2004).
26. N. J. Mantua, S. R. Hare, Y. Zhang, J. M. Wallace, R. C. Francis, *Bull. Am. Meteorol. Soc.* **78**, 1069 (1997).
27. W. T. Peterson, F. B. Schwing, *Geophys. Res. Lett.* **30**, 1896 (2003).
28. J. Chen, A. D. Del Genio, B. E. Carlson, M. G. Bosilovich, *J. Clim.* **21**, 2634 (2008).
29. R. J. Burgman, A. C. Clement, C. M. Mitas, J. Chen, K. Esslinger, *Geophys. Res. Lett.* **35**, L01704 (2008).
30. Y. Zhang, J. M. Wallace, D. S. Battisti, *J. Clim.* **10**, 10041020 (1997).
31. R. Seager, M. Benno Blumenthal, Y. Kushnir, *J. Clim.* **8**, 1951 (1995).
32. W. Hazeleger, R. Seager, M. Cane, N. Naik, *J. Phys. Oceanogr.* **34**, 320 (2004).
33. J. R. Norris, *J. Geophys. Res. Atmos.* **110**, D21110 (2005).
34. C.-C. Ma, C. R. Mechoso, A. W. Robertson, A. Arakawa, *J. Clim.* **9**, 1635 (1996).
35. Y. Wang, S.-P. Xie, B. Wang, H. Xu, *J. Clim.* **18**, 934 (2005).
36. S. Nigam, *J. Clim.* **10**, 2447 (1997).
37. V. Misra, L. Marx, *J. Geophys. Res.* **112**, D20105 (2007).
38. G. A. Meehl *et al*., *Bull. Am. Meteorol. Soc.* **88**, 1383 (2007).
39. We only include the 18 (of 23) models for which all of the diagnostics used in this study are available.
40. E. M. Volodin, N. A. Dianskii, *Russ. Meteorol. Hydrol.* **12**, 1 (2004).
41. T. C. Johns *et al*., *J. Clim.* **19**, 1327 (2006).
42. A. P. Lock, A. R. Brown, M. R. Bush, G. M. Martin, R. N. B. Smith, *Mon. Weather Rev.* **128**, 3187 (2000).
43. G. A. Vecchi, B. J. Soden, *J. Clim.* **20**, 4316 (2007).
44. M. Zhang, H. Song, *Geophys. Res. Lett.* **33**, L12701 (2006).
45. R. L. Miller, *J. Clim.* **10**, 409 (1997).
46. B. Medeiros *et al*., *J. Clim.* **21**, 4974 (2008).

47. We gratefully acknowledge comments from B. Stevens and two anonymous reviewers. We also acknowledge the various international modeling groups participating in IPCC/AR4, the Program for Climate Model Diagnosis and Intercomparison (PCMDI), and the IPCC Data Archive at Lawrence Livermore National Laboratory (supported by the Office of Science, U.S. Department of Energy) for providing the data that made this analysis possible. Funding for this work was provided by the National Oceanic and Atmospheric Administration Office of Global Programs (grant NA06OAR4310142). An NSF CAREER award (ATM02-38527) supported the work by J.R.N.

Supporting Online Material

www.sciencemag.org/cgi/content/full/325/5939/460/DC1
SOM Text
Figs. S1 to S5
References

22 January 2009; accepted 11 June 2009
10.1126/science.1171255

The Dynamics of Phenotypic Change and the Shrinking Sheep of St. Kilda

Arpat Ozgul,[1] Shripad Tuljapurkar,[2] Tim G. Benton,[3] Josephine M. Pemberton,[4] Tim H. Clutton-Brock,[5] Tim Coulson[1]*

Environmental change, including climate change, can cause rapid phenotypic change via both ecological and evolutionary processes. Because ecological and evolutionary dynamics are intimately linked, a major challenge is to identify their relative roles. We exactly decomposed the change in mean body weight in a free-living population of Soay sheep into all the processes that contribute to change. Ecological processes contribute most, with selection—the underpinning of adaptive evolution—explaining little of the observed phenotypic trend. Our results enable us to explain why selection has so little effect even though weight is heritable, and why environmental change has caused a decline in the body size of Soay sheep.

A major goal of population biology is to understand how environmental change generates a rapid phenotypic response (*1*, *2*). Recently, it has been recognized that evolution can occur on ecological time scales (*2*), and the new challenge is to differentiate trait dynamics driven by evolution from those driven by ecological responses to environmental change (*3*). This is difficult because ecological and evolutionary effects are intimately intertwined (*2*, *4*), and available analytical methods do not allow the quantification of different sources of change. For example, evolutionary models of phenotypic change (*5*, *6*) focus on selection and the genetic response to it (*7*). However, when applied in well-studied, pedigreed, wild animal populations, they often fail to explain phenotypic outcome, leading many authors to speculate that plastic responses to environmental variation play a large role in phenotypic dynamics (*1*, *8*–*11*). Conversely, some phenotypic trends are interpreted as evolutionary change without any evolutionary analysis. An exact method to decompose phenotypic change into contributing processes would aid in identifying the roles of selection (the underpinning of adaptive evolution) and ecology in generating phenotypic trends.

In 1970, Price developed an equation that describes change in the mean value of a phenotypic

[1]Department of Life Sciences, Imperial College London, Silwood Park, Ascot, Berkshire SL5 7PY, UK. [2]Department of Biology, Stanford University, Stanford, CA 94305-5020, USA. [3]Faculty of Biological Sciences, University of Leeds, Leeds LS2 9JT, UK. [4]Institute for Evolutionary Biology, University of Edinburgh, Kings Buildings, West Mains Road, Edinburgh EH9 3JT, UK. [5]Department of Zoology, University of Cambridge, Downing Street, Cambridge CB2 3EJ, UK.

*To whom correspondence should be addressed. E-mail: t.coulson@imperial.ac.uk